Theory of Tribovoltaics: Direct Current Generation at a *p-n* Semiconductor Interface

Morten Willatzen,[1,2,*] Zhiwei Zhang,[1,2] and Zhong Lin Wang[1,2,3]

[1] *Beijing Institute of Nanoenergy and Nanosystems, Chinese Academy of Sciences, Beijing 100083, China*
[2] *School of Nanoscience and Technology, University of Chinese Academy of Sciences, Beijing 100049, China*
[3] *Georgia Institute of Technology, Atlanta, Georgia 30332-0245, USA*

(Received 22 September 2023; revised 22 December 2023; accepted 22 January 2024; published 20 February 2024; corrected 3 May 2024)

A simple theory of tribovoltaics is proposed by using a quantum mechanical model of energy release due to sliding-induced bonding between the surfaces of a *p*-doped semiconductor and a *n*-doped semiconductor. The energy release in forming a bond may lead to the excitation of electron-hole pairs at the *p-n* semiconductor interface if the released energy is higher than the effective band gap at the semiconductor interface. An expression for the generated current as a function of the relative sliding speed between the *p* and *n* sides is suggested and used to model current transport by solving the complete set of drift-diffusion equations with appropriate boundary and initial conditions. Analytical results are obtained and verified numerically using the COMSOL finite-element-method software. It is shown that since the typical time period associated with periodic sliding is many orders of magnitude higher than the carrier lifetimes, the time-dependent variations in the electron and hole concentrations and the current density follow the time variation of the sliding speed. Since the electron-hole pair generation occurs near the semiconductor interface only, the current density is shown to be constant as a function of position even if the sliding speed changes in time.

DOI: 10.1103/PRXEnergy.3.013009

I. INTRODUCTION

The search for new types of green and energy-efficient harvesting mechanisms continues at a high pace due to the shortage of fossil energy and global climate change. Triboelectric nanogenerators (TENGs) are important green-harvesting candidates. Here, the traditional layout (ac TENGs) is that two or more dielectric layers move with respect to one another in a periodic fashion, generating alternating currents by virtue of a time-changing electric displacement [1–7]. A new type of TENG, the dc TENG, has been proposed recently, where the sliding of two materials leads to the generation of electron-hole pairs at the interface due to energy release from bonding formation between surface states associated with the isolated sliding materials [8–12]. Many designs of dc TENGs have been suggested based on, e.g., semiconductor-semiconductor, metal-semiconductor, semiconductor-insulator-semiconductor, and metal-insulator-semiconductor structures [13]. For doped *p-n* semiconductor structures, the generated electrons and holes are accelerated in opposite directions by the built-in electric field, independent of the sliding speed and the sliding direction. The generated current is therefore dc. The dc TENGs fill an important gap in the portfolio of existing harvesting devices due to their generation of high-current-density (dc) output signals and simple structure designs. While experimental realizations of dc TENGs have been demonstrated recently, the theoretical understanding of the mechanism behind electron-hole pair generation due to sliding is still not well understood [14–17].

At the present time, the numerical and analytical solutions of drift-diffusion equations receive much attention in, e.g., the study of organic semiconductors [18–21] and solar-cell applications [22,23]. Many of the recent applications [24] are based on classical semiconductor drift-diffusion numerical methods [25–27].

We propose a simple quantum mechanical model for the energy release in forming bonds between two surface states associated with the isolated materials. With a certain efficiency, if the energy released in forming bonds (the energy quantum is known as the "bindington") is higher than the effective band gap at the semiconductor interface between the sliding materials, electron-hole pairs may be excited. This effect is modeled in the current transport

*mortenwillatzen@binn.cas.cn

equations by the use of a carrier-generation term described by a delta function at the semiconductor interface. The output dc current is calculated analytically and verified numerically using the COMSOL finite-element software for the case of a general time-dependent sliding speed.

II. SEMICONDUCTOR *p-n* EQUATIONS

The tribovoltaic effect is well known, yet the theory is not fully understood [8–11]. A one-dimensional theory is proposed for the current generation due to tribovoltaics based on the semiconductor equations applied to *p-n* structures (Figs. 1 and 2). The three differential equations are the Poisson equation and the two current continuity equations,

$$\frac{\partial^2\phi}{\partial x^2} = -\frac{\rho}{\epsilon}, \tag{1}$$

$$\frac{\partial n}{\partial t} = \frac{1}{q}\frac{\partial J_n}{\partial x} + G_n - R_n, \tag{2}$$

$$\frac{\partial p}{\partial t} = -\frac{1}{q}\frac{\partial J_p}{\partial x} + G_p - R_p, \tag{3}$$

where n and p are the electron and hole concentrations, ϕ is the electrostatic potential, J_n (J_p) is the electron (hole) current density, G_n (G_p) is the electron (hole) generation rate, R_n (R_p) is the electron (hole) recombination rate, ρ is the charge density, and ϵ is the material permittivity. Variables x and t are the spatial and time coordinates, respectively, and q is the positive elementary charge. Using a drift-diffusion current-density-model assumption,

$$J_n = qD_n\frac{\partial n}{\partial x} + q\mu_n n\mathcal{E}, \tag{4}$$

$$J_p = -qD_p\frac{\partial p}{\partial x} + q\mu_p p\mathcal{E}. \tag{5}$$

Eqs. (1)–(3) become [28]

$$\frac{\partial^2\phi}{\partial x^2} = \frac{q}{\epsilon}\left(N_A(x) - N_D(x) + n - p\right), \tag{6}$$

$$\frac{\partial n}{\partial t} = n\mu_n\frac{\partial\mathcal{E}}{\partial x} + \mu_n\mathcal{E}\frac{\partial n}{\partial x} + D_n\frac{\partial^2 n}{\partial x^2} + G_n - R_n, \tag{7}$$

$$\frac{\partial p}{\partial t} = -p\mu_p\frac{\partial\mathcal{E}}{\partial x} - \mu_p\mathcal{E}\frac{\partial p}{\partial x} + D_p\frac{\partial^2 p}{\partial x^2} + G_p - R_p, \tag{8}$$

where $\mathcal{E} = -\partial\phi/\partial x$ is the electric field, N_A (N_D) is the acceptor (donor) concentration, μ_n (μ_p) is the electron (hole) mobility, and D_n (D_p) is the electron (hole) diffusivity. In writing these equations, we have assumed that the materials forming the p and n sides are the same except for differences in the doping concentrations as indicated in Eq. (6) by writing $N_A(x)$ and $N_D(x)$. The driving mechanism behind tribovoltaics originates from generation rates G_n and G_p, which depend on the nature of contact electrification. This model will be examined in Sec. III.

The above set of equations constitutes three second-order differential equations in space. Hence, for *each* dependent variable n, p, and ϕ, two boundary conditions are required [28],

$$p \text{ side:} \quad p(x = x_L) = N_A, \quad n(x = x_L) = \frac{n_i^2}{N_A},$$
$$\phi(x = x_L) = 0, \tag{9}$$

$$n \text{ side:} \quad n(x = x_R) = N_D, \quad p(x = x_R) = \frac{n_i^2}{N_D},$$
$$\phi(x = x_R) = \phi_{\text{bi}} - V_{\text{apl}}, \tag{10}$$

where n_i is the intrinsic carrier density, V_{apl} is the applied voltage, and ϕ_{bi} is the built-in potential,

$$\phi_{\text{bi}} = \frac{k_B T}{q}\ln\left(\frac{N_A N_D}{n_i^2}\right), \tag{11}$$

where T is the temperature and k_B is Boltzmann's constant. Subject to the initial values of n, p, and ϕ, the above set of equations constitutes a complete model framework. However, it is only in a limited set of cases that analytical solutions can be found. Otherwise, a numerical solution must be sought. In this work, all numerical results are based on COMSOL finite-element calculations, where Eqs. (6)–(8) are solved subject to the boundary conditions given in Eqs. (9) and (10).

III. TRIBOVOLTAIC MODEL FOR STEADY-STATE CURRENT GENERATION

In this section, the two situations in which the sliding speed is constant in time and varying in time are discussed in Secs. III A and III B, respectively.

A. Tribovoltaic model current generation due to a constant-in-time sliding speed

A simple analytical steady-state model for tribovoltaics can now be formulated by assuming that sliding of the p-side material against the n-side material leads to a localized electron-hole pair generation,

$$G_n = G_p = \tilde{G}\delta(x), \tag{12}$$

where $\tilde{G}$ is a function describing the nature of contact electrification and $\delta(x)$ is a delta function in space centered at the semiconductor interface $x = 0$. We consider

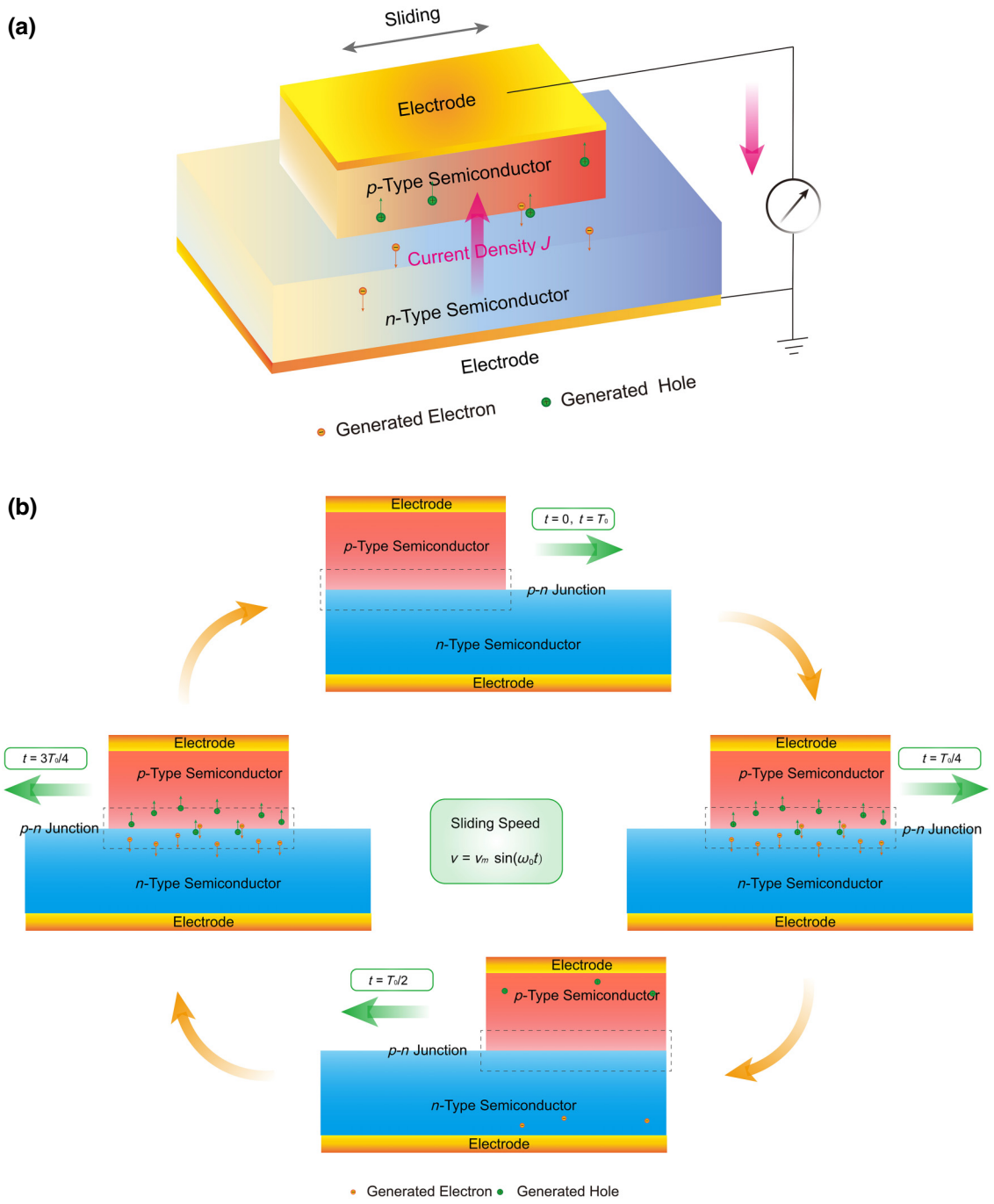

FIG. 1. (a) A three-dimensional schematic drawing of a tribovoltaics p-n semiconductor interface device. (b) A schematic drawing of a sinusoidally driven tribovoltaic cycle in a p-n structure invoked by the relative movement of the p layer with respect to the n layer. The frequency of the sliding f is related to the sliding period T_0 and ω_0 as $f = 1/T_0 = \omega_0/(2\pi)$. As the p layer moves relative to the n layer, electron-hole pairs are generated at the semiconductor interface. The generation rate is a function of the relative speed between the two layers. Once an electron-hole pair is generated, the electron (hole) moves toward the electrode on the n side (p side). The tribovoltaic current can be harvested in an external circuit.

that the parameter $\tilde{G}$ can be written as a function of the sliding speed v (assumed positive) multiplied by a material-dependent function T_m, i.e.,

$$\tilde{G} = f(v)T_m, \tag{13}$$

if charging due to contact electrification is assumed to be proportional to the sliding speed. The quantity T_m must be determined from quantum mechanics, electronic band structure, and molecular-bonding properties [29]. In the steady state, and in the absence of a bias voltage across the structure, from Eqs. (2) and (3), the triboelectric currents

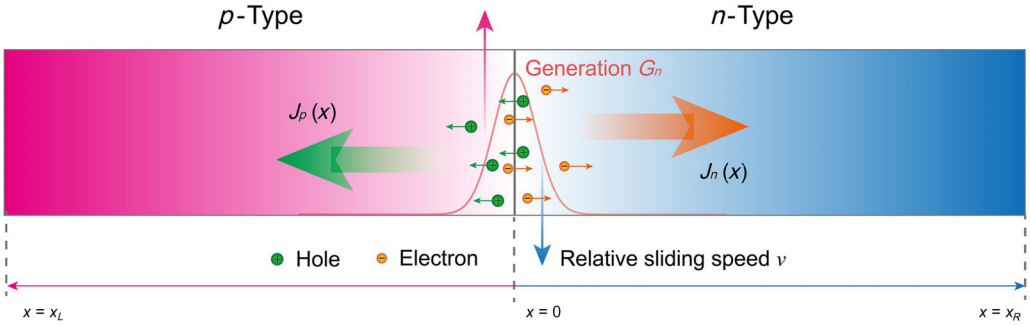

FIG. 2. Electron-hole pair generation at the semiconductor interface due to the sliding of a p-doped semiconductor on a n-doped semiconductor.

reduce to

$$\frac{dJ_n^T}{dx} = -qG_n = -q\tilde{G}\delta(x), \tag{14}$$

$$\frac{dJ_p^T}{dx} = qG_p = q\tilde{G}\delta(x). \tag{15}$$

Thus,

$$\int_{-\infty}^{x} \frac{dJ_n^T}{dx}dx = J_n^T(x) - J_n^T(-\infty) = J_n^T(x) = \int_{-\infty}^{x} -q\tilde{G}\delta(x)dx = -q\tilde{G}H(x), \tag{16}$$

$$\int_{x}^{\infty} \frac{dJ_p^T}{dx}dx = J_p^T(\infty) - J_p^T(x) = -J_p^T(x) = \int_{x}^{\infty} q\tilde{G}\delta(x)dx = q\tilde{G}(1 - H(x)), \tag{17}$$

where the Heaviside function $H(x)$ has been introduced [$H(x) = 1$ if $x > 0$ and $H(x) = 0$ if $x < 0$] and $J_n^T(-\infty) = J_p^T(\infty) = 0$.

Finally, the total current density due to tribovoltaics generation becomes

$$J^T(x) = J_n^T(x) + J_p^T(x) = -q\tilde{G}H(x) + q\tilde{G}(H(x) - 1) = -q\tilde{G}, \tag{18}$$

which is constant (independent of x). Note that in the absence of an applied voltage, the total current density is simply equal to J^T. The total tribovoltaic current in the reverse direction is, therefore, $I^T = J^T A = q\tilde{G}A$, where A is the cross-section area of the p-n structure, which can be harvested through an external resistance R.

B. Tribovoltaic model current generation due to a time-dependent sliding speed

If the sliding speed changes in time, the generation rate becomes

$$G_n = G_p = \tilde{G}(t)\delta(x). \tag{19}$$

Since the time variation of sliding is slow—say, in the order of a second—the terms $\partial n/\partial t$ and $\partial p/\partial t$ on the left-hand side of the continuity equations are negligible compared to, e.g., the recombination term n/τ_n (or p/τ_p), as the latter involves carrier lifetimes τ_n (τ_p) in the range of one microsecond or less. Hence, the analysis in the preceding section can be repeated, i.e.,

$$J^T(x,t) = J_n^T(x,t) + J_p^T(x,t) = -q\tilde{G}(t)H(x) + q\tilde{G}(t)(H(x) - 1) = -q\tilde{G}(t), \tag{20}$$

which is independent of x. So the tribovoltaic current density follows the time dependence of the generation rate. Again, since the triboelectric-generated carrier concentrations are orders of magnitude smaller than the background doping concentrations, the electric field can be considered independent of time in the depletion zone and zero in the neutral regions. Thus, the electron and hole concentrations must follow the same time variation as the electron and hole current densities, respectively. Detailed numerical results using COMSOL confirm this behavior.

IV. ENERGY RELEASE FROM BONDING OF SURFACE ATOMS

Consider two surface atoms in materials A and B, respectively (see Fig. 3). The use of a one-electron model allows us to write, for the one-dimensional Hamiltonian of an electron moving in the combined surface potential of

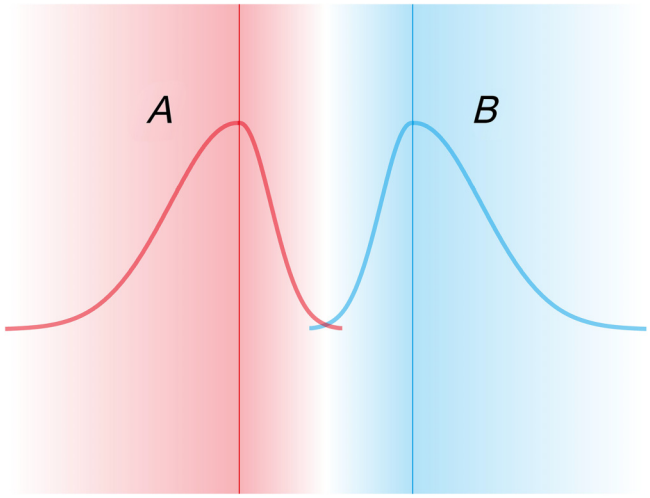

FIG. 3. A schematic drawing of the surface states in isolated materials A (left) and B (right). As materials A and B approach each other, the surface states begin to overlap and bonding states are formed. The z axis is oriented perpendicular to the surface planes. The left and right potentials correspond to V_A and V_B, respectively. It is known from the theory of surface states and empirical tight-binding theory [30] that surface eigenstates decay exponentially either in a monotonous fashion or oscillating into the bulk region. Away from the crystal, eigenstates decay in a monotonous fashion and typically with a stronger decay rate than into the bulk.

materials A and B,

$$H = \frac{p_z^2}{2m_0} + V_A(z - z_A) + V_B(z - z_B), \tag{21}$$

where m_0 is the free-electron mass and $V_A(z - z_A)$ is the potential centered at $z = z_A$, where the latter defines the surface position of material A. Similarly, $V_B(z - z_B)$ is the potential centered at $z = z_B$, where the latter defines the surface position of material B. Hence, the surfaces of materials A and B are in the x-y plane and z denotes the position of the electron in the direction perpendicular to the material surfaces. The detailed quantum mechanical theory for computing bonding energies between two different materials A and B is given in Appendix C.

A. Bonding between similar materials

In the case in which materials A and B are the *same* material, we have, with reference to the model details and parameters in Appendix C,

$$\begin{aligned} \psi_A &= \psi_B, \\ V_A &= V_B = V, \\ E_A &= E_B = E, \end{aligned} \tag{22}$$

$$\begin{aligned} r_{AB} &= r_{BA} = r, \\ S_{ABA} &= S_{BAB} = s, \\ t_{AAB} &= t_{BAA} = t_{BBA} = t_{ABB} = t, \end{aligned}$$

and the energy eigenvalues in Eq. (C22) become,

$$\mathcal{E} = E \mp \frac{t}{1 \mp r} + \frac{s}{1 \mp r}. \tag{23}$$

If the overlap r is much smaller than 1 (which, however, is typically not a good approximation if the two materials are forced atomically close in a tribovoltaic situation), the latter expression for the bonding-energy eigenvalues simplifies further, to

$$\mathcal{E} = E \mp t + s. \tag{24}$$

It should be emphasized that from empirical tight-binding theory, it is known that the shift (s) and transfer (t) integrals are both negative, while the overlap integral r is positive [31]. Hence, at least one of the bonding states (with energy $\mathcal{E} = E + t + s$) is energetically below the energy of a surface electron in an isolated material (Fig. 4). The formation of such a bond between materials A and B by a surface electron leads to the release of energy, which may be used to excite an electron-hole pair of relevance for tribovoltaics. An approximation for the transfer integral t is

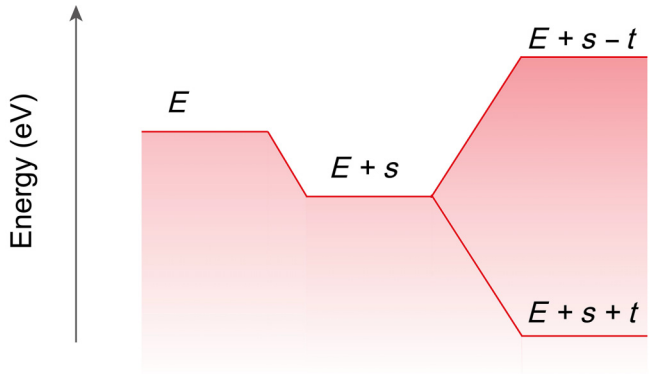

FIG. 4. A schematic drawing of the electron energy levels when two surface atoms in identical materials A and B form a bond, assuming the overlap integral $r \ll 1$ such that Eq. (24) applies. Note that the shift s and transfer t integrals are both negative, while the overlap integral r is positive. There is therefore always one bonding level with energy $E + s + t$ below the energy E of a surface electron on the isolated materials A or B. An electron occupying such a bonding level can lead to the excitation of an electron-hole pair (tribovoltaics) if the energy difference $E - (E + s + t) = -s - t$ is larger than the effective band gap $E_c(z = 0) - E_v(z = 0)$ at the semiconductor interface $z = 0$.

to use Harrison's universal hopping parameters [32,33],

$$t = -1.32\frac{\hbar^2}{md^2}, \tag{25}$$

where m is the effective mass and d is the bond length for the solid.

B. Example: Calculation of bonding energy and energy release due to surface coupling between two identical materials

Consider the following parameter values corresponding to two GaAs surfaces in contact [34, Table 2.3, p. 55]:

$$\begin{aligned} &t = t_{AAB} = t_{BAA} = t_{BBA} = t_{ABB} = V_{ss\sigma} = -1.79 \text{ eV}, \\ &r = r_{AB} = r_{BA} = 0.2, \\ &s = s_{ABA} = s_{BAB} \approx rt = -0.358 \text{ eV}, \end{aligned} \tag{26}$$

where $V_{ss\sigma}$ is the interatomic matrix element between two surface states of S type and the overlap integral r is considered to be 0.2 (note that the overlap integral value can be any value between 0 and 1, depending on the distance between the two surfaces in contact). The energy release in forming a low-energy bonding state is then

$$\Delta\mathcal{E} \approx -(t+s) = 2.148 \text{ eV},$$

according to Eq. (24). Hence, the formation of a bonding state may lead to the excitation of an electron-hole pair, since 2.148 eV is above the effective band gap $E_c(0) - E_v(0)$ at the p-n semiconductor interface (the band gap of bulk GaAs is 1.424 eV). A similar calculation for Si with $V_{ss\sigma} = -1.93$ eV and $r = 0.2$ leads to an energy release of 2.316 eV, which is substantially higher than the indirect band gap of Si (1.1 eV). Hence, bond formation may lead to electron-hole pair generation for two of the most important p-n–junction materials.

V. CURRENT DENSITY VERSUS SLIDING SPEED: EXPERIMENTAL DATA AND NUMERICAL RESULTS

In Fig. 5, experimental data from Ref. [35, Fig. 1] are reproduced for the short-circuit current as a function of the sliding speed. It is evident that the current density has a substantial linear component as a function of the sliding speed but a linear relationship is not exact. Hence, the choice of a general function $f(v)$ to describe the relationship between the sliding speed and the current density is better justified than just assuming a linear dependence.

In the numerical calculations that follow, we use the data in Table I and, for simplicity, assume that the electron-hole pair-generation rate is a linear function of the sliding speed $G = G_n = G_p = f(v)T_m = \gamma v T_m$.

In Fig. 6, the quasi-Fermi levels and the carrier densities are plotted as a function of position for three values of the sliding speed: $v = 0, v = 0.01$ m/s, and $v = 0.1$ m/s. Note that the changes in carrier densities due to

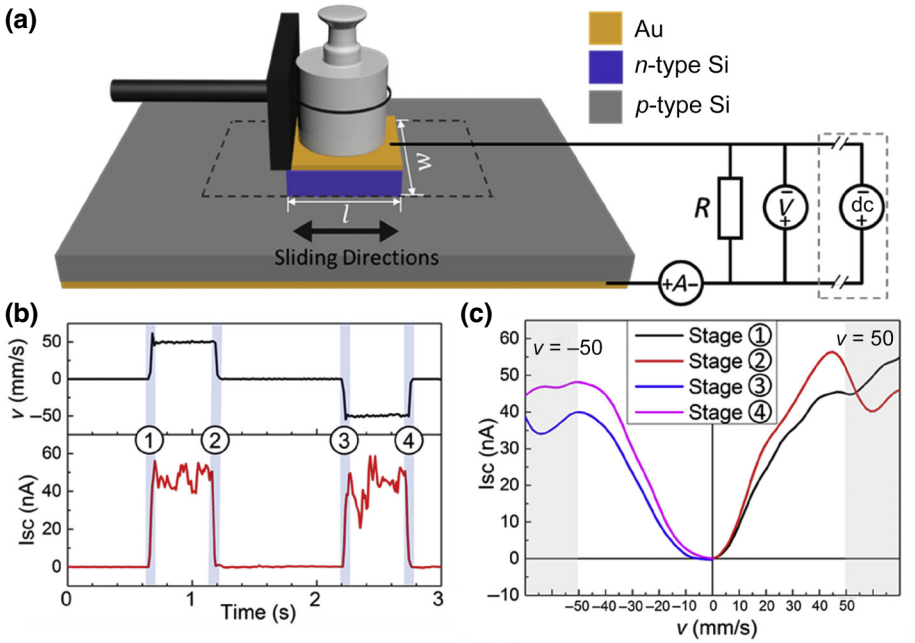

FIG. 5. Experimental data for the short-circuit current density versus the sliding speed. The data are from Ref. [35, Fig. 1]. (a) The measurement setup. (b) The short-circuit current (Isc) as a function of time. (c) An enlargement of the short-circuit current versus the sliding speed for the four stages 1–4.

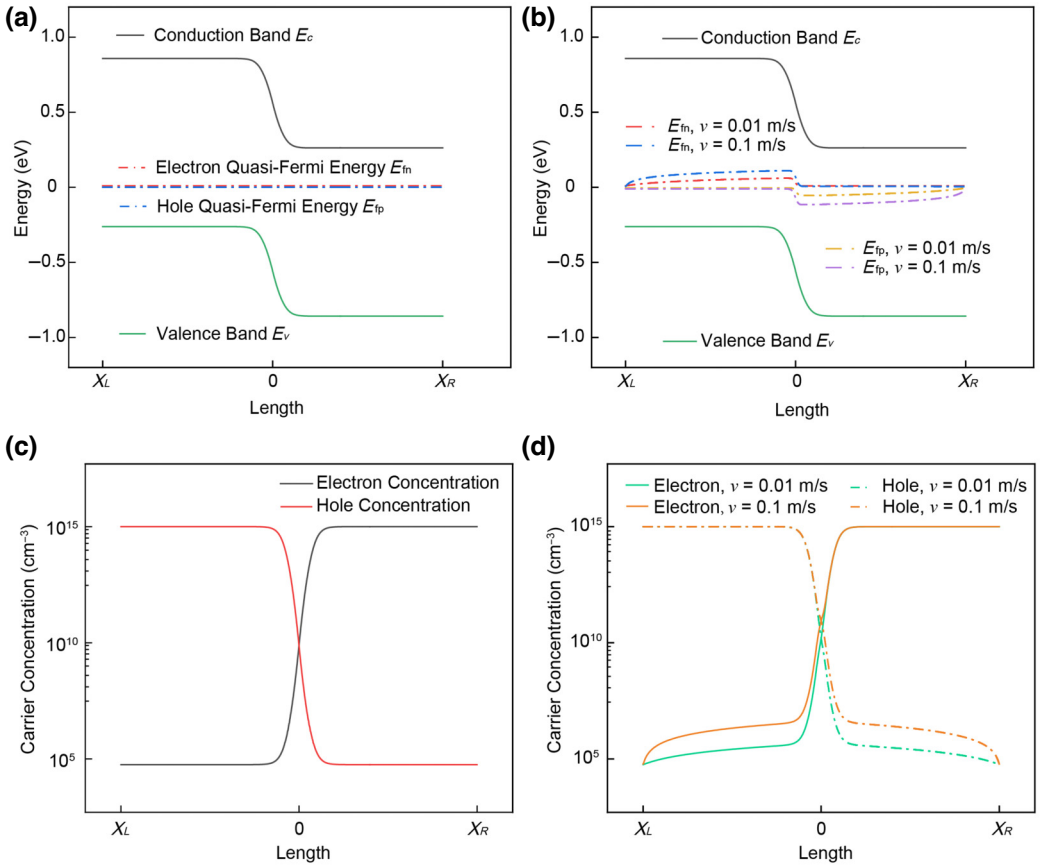

FIG. 6. (a),(b) The electron and hole quasi-Fermi energies as a function of position (GaAs). The generation rates G_n and G_p are assumed to be linear functions of the sliding speed. (c),(d) The electron and hole carrier concentrations as a function of position. The left-hand plots [(a) and (c)] correspond to a zero sliding speed. The right-hand plots [(b) and (d)] show the same but for two different sliding speeds. The parameter values are as follows: $\gamma = 1 \times 10^5$ m^{-1}, $a = 5.64 \times 10^{-10}$ m, $\tilde{\eta}_{eh\,\mathrm{pair}} = 1$, and $\kappa = 2$. The results are obtained numerically in COMSOL by solving the full set of drift-diffusion equations [Eqs. (6)–(8)] and boundary conditions [Eqs. (9) and (10)], using the parameter values listed in Table I. Note that the numerical results correspond to boundary positions $x_R = -x_L = L$.

electron-hole pair generation are negligibly small compared to the background doping concentrations of 10^{15} cm^{-3}.

In Fig. 7, the electron and hole current densities are plotted as a function of position for a sliding speed of 0.01 m/s. The numerical results confirm that the current density $J(x) = J_n(x) + J_p(x)$ is independent of position and nonzero due to sliding-induced electron-hole pair generation at the p-n semiconductor interface.

In Fig. 8, the generated current density is shown as a function of the sliding speed v for different γ values.

VI. GENERATION OF ELECTRON-HOLE PAIRS DUE TO SLIDING

In this section, we shall attempt to make a model for the generation rate of an electron-hole pair due to the sliding of two materials against one another. Let us assume that the energy released by a surface electron in forming a bond between two materials can lead to several processes (denoted X), each characterized by an efficiency η_X, i.e.,

$$1 = \eta_{\mathrm{kin},e} + \eta_{\mathrm{kin},h} + \eta_{\mathrm{photon}} + \eta_{\mathrm{phonon}} + \eta_{eh\,\mathrm{pair}} + \ldots. \tag{27}$$

where $\eta_{\mathrm{kin},e}$ ($\eta_{\mathrm{kin},h}$) is the probability that the energy released in forming the bond adds to the kinetic energy of another electron (hole), η_{photon} (η_{phonon}) is the probability that the energy released leads to emission of a photon (phonon), and $\eta_{eh\,\mathrm{pair}}$ is the probability that the energy released is used to create an electron-hole pair. It is the latter process that contributes to the tribovoltaic effect. If the energy released in forming a bond, $E_A - \mathcal{E}$ (or $E_B - \mathcal{E}$) is larger than the effective band gap ($E_g^{\mathrm{eff}} = E_c(z=0) - E_v(z=0)$) at the interface ($z = 0$) between materials A and B, an electron-hole pair excitation at the interface is energetically allowed. Hence, we can write

$$\eta_{eh\,\mathrm{pair}} = \tilde{\eta}_{eh\,\mathrm{pair}} H[E_{B(A)} - \mathcal{E} - (E_c(z=0) - E_v(z=0))], \tag{28}$$

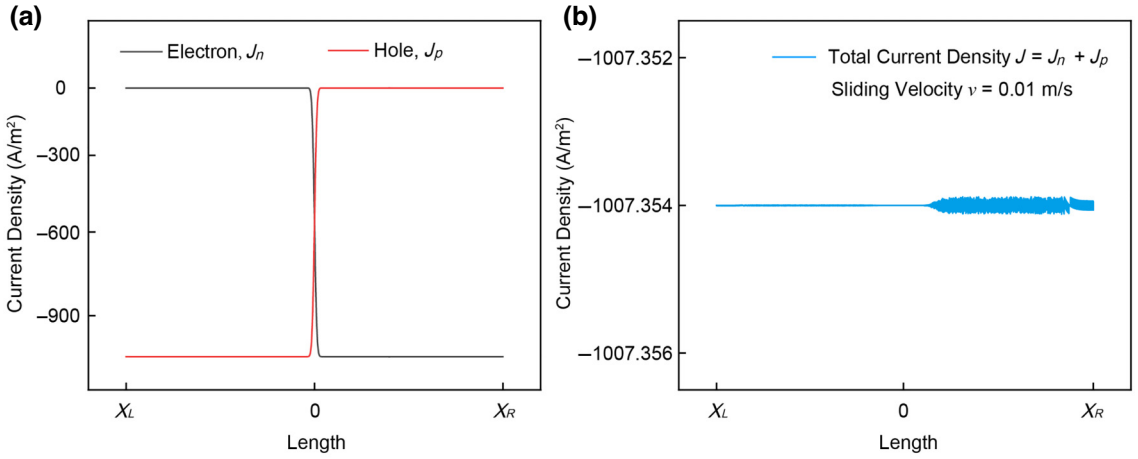

FIG. 7. The current density as a function of position calculated numerically for a sliding speed of 0.01 m/s (GaAs). (a) Current densities J_n and J_p as a function of position. (b) The total current density, $J = J_n + J_p$, as a function of position. The parameter values are as follows: $\gamma = 1 \times 10^5$ m^{-1}, $a = 5.64 \times 10^{-10}$ m, $\tilde{\eta}_{eh\,\mathrm{pair}} = 1$, and $\kappa = 2$. The results are obtained numerically in COMSOL by solving the full set of drift-diffusion equations [Eqs. (6)–(8)] and boundary conditions [Eqs. (9) and (10)], using the parameter values listed in Table I. Note that the numerical results correspond to boundary positions $x_R = -x_L = L$.

where $H[\cdot]$ is the Heaviside function. The introduction of the Heaviside function ensures that electron-hole pair generation is possible only if it is energetically allowed.

The total number of generated electron-hole pairs per volume per unit time due to bonding between two materials can now be written as

$$N_{eh\,\mathrm{pair}} = N_{\mathrm{surface\ atoms}} \times P_{\mathrm{bond}} \times \eta_{eh\,\mathrm{pair}} \times \delta(x), \tag{29}$$

$$N_{eh\,\mathrm{pair}} = G = \tilde{G}\delta(x), \tag{30}$$

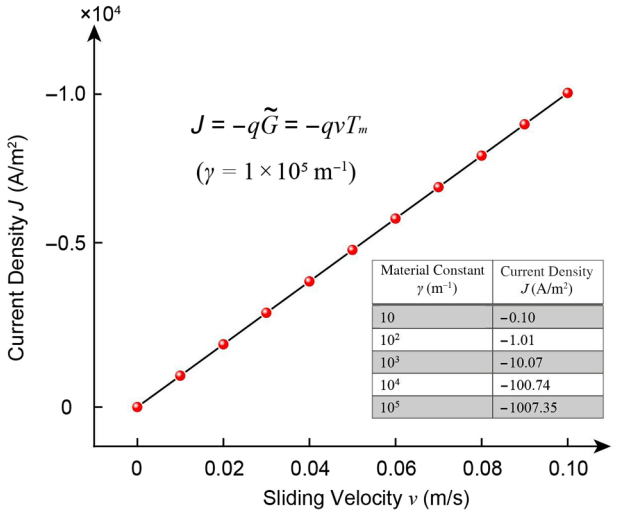

Material Constant γ (m^{-1})	Current Density J (A/m^2)
10	−0.10
10^2	−1.01
10^3	−10.07
10^4	−100.74
10^5	−1007.35

FIG. 8. The calculated current density as a function of the sliding speed (GaAs). The current density at a sliding speed of 0.01 m/s is shown in the inset table for different γ parameters. Other parameters are as follows: $a = 5.64 \times 10^{-10}$ m, $\tilde{\eta}_{eh\,\mathrm{pair}} = 1$, and $\kappa = 2$. The results are obtained numerically in COMSOL by solving the full set of drift-diffusion equations [Eqs. (6)–(8)] and boundary conditions [Eqs. (9) and (10)], using the parameter values listed in Table I.

where $N_{\mathrm{surface\ atoms}}$ is the number of surface-atom pairs per unit area formed between material A and B, which, assuming nearest-neighbor couplings only, is equal to the number of surface atoms on material A (or material B). P_{bond} is the probability per unit time per surface atom in material A to form a bond with a B surface atom *due to sliding*, which we model as

$$P_{\mathrm{bond}} = f(v), \tag{31}$$

where f is a function that depends on the sliding speed v between the two materials. The most general model is to consider f to be a general function of the sliding speed v. Mathematically, assuming the electron-hole pair generation to be a smooth function of the sliding speed, $f(v)$ can be represented by a Taylor series in v. Hence, at low sliding speeds the linear term dominates, while at higher sliding speeds higher-order terms of $f(v)$ begin to contribute. This behavior is indeed justified by the experimental results in Ref. [35], shown in Fig. 5: at low sliding speeds, the current increases in an approximately linear fashion. As the sliding speed increases, the experimental results in Fig. 5 reveal that current saturation gradually sets in. While the precise physical details behind the function $f(v)$ in general, and the saturation phenomenon in particular, are unknown and beyond the scope of the present work, we attribute the current saturation effect to the build-up of an opposing Coulomb field due to the generated carriers as well as an increase in carrier recombination as the electron-hole pair-generation rate increases.

To simplify the analysis and case study below, we now choose to approximate the function $f(v)$ by the first linear

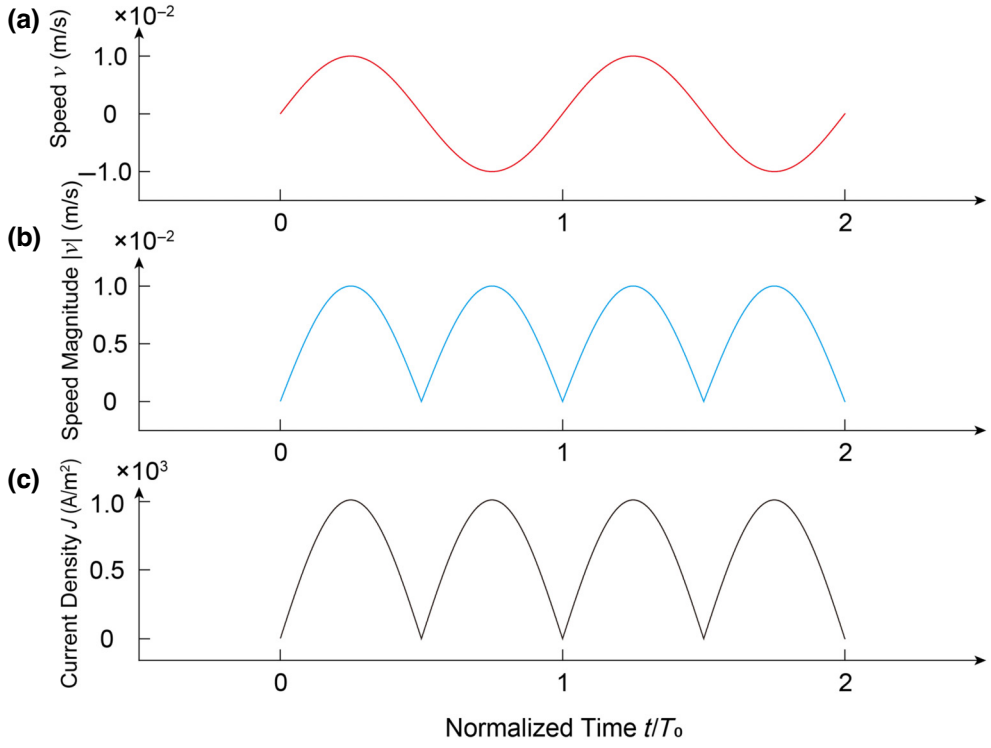

FIG. 9. (a),(c) For (a) a specified sinusoidal time dependence of the sliding velocity, (c) the calculated time-dependent plot of the positive current density for GaAs. (b) The absolute value of the sliding speed. The results are obtained numerically in COMSOL by solving the full set of drift-diffusion equations [Eqs. (6)–(8)] and boundary conditions [Eqs. (9) and (10)], using the parameter values listed in Table I.

term in its expansion, since this term dominates at low sliding speeds.

If the two materials are assumed to have simple cubic lattices, the number of surface atoms per unit area for each material, $N_{\text{surface atoms}}$, can be approximated as $\kappa/A_{\text{u.c.}} = \kappa/a^2$, where κ is a crystal structure factor equal to 1 for the simple cubic lattice, $A_{\text{u.c.}}$ is the surface area of one facet of the unit cell (in material A, the facet that fronts the surface of material B), and a is the lattice constant (assumed to be the same for the two materials). Generally, for cubic lattices,

$$\kappa = \begin{array}{ll} 1, & \text{simple cubic lattice,} \\ 1, & \text{body-centered cubic lattice,} \\ 2, & \text{face-centered cubic lattice.} \end{array} \tag{32}$$

Combining the above equations, Eqs. (28)–(31), with Eq. (13) gives an expression for the functions T_m and $\tilde{G}$,

$$\begin{aligned} T_m &= \kappa/a^2 \times \tilde{\eta}_{eh\,\text{pair}} \\ &\quad \times H[E_{B(A)} - \mathcal{E} - (E_c(z=0) - E_v(z=0))], \\ \tilde{G} &= f(v) T_m, \end{aligned} \tag{33}$$

that appears in the equation for the electron-hole pair-generation rate G in the transport equations. We note that $E_{B(A)} - \mathcal{E}$ is the energy release due to bonding that was calculated in Sec. V and $E_c(z=0) - E_v(z=0)$ is the effective band gap at $z = 0$. The latter can be calculated, e.g., by using the $\mathbf{k}\cdot\mathbf{p}$ method [36], to solve the drift-diffusion equations for a p-n structure of known semiconductor materials. Finally, we note that the unknown parameters $0 \le \tilde{\eta}_{eh\,\text{pair}} \le 1$ and γ must be determined experimentally.

Observe that the analytical result for the current density, assuming a linear relationship between the current density and the sliding velocity and using the data in Table I, is, in the case of GaAs,

$$\begin{aligned} J^T &= -q\tilde{G} = -qf(v)T_m = -q\gamma v T_m = -q\gamma v \frac{\kappa}{a^2}\tilde{\eta}_{eh\,\text{pair}} \\ &= -1.602 \times 10^{-19} \times 1 \times 10^5 \times 0.01 \\ &\quad \times \frac{2}{(5.64 \times 10^{-10})^2} \times 1 \\ &= -1007\ \text{A/m}^2, \end{aligned} \tag{34}$$

which is in perfect agreement with the numerical result in Fig. 7. The inset table in Fig. 8 shows the current density for different γ values.

A time-dependent COMSOL calculation of the nonlinear drift-diffusion equations has also been carried out,

assuming that the sliding speed is a sinusoidal function of time. Figure 9 reveals that, indeed, the current density follows the exact same time dependence as the sliding speed [calculated as the absolute value of the sliding velocity—compare Figs. 9(b) and 9(c)]. This numerical result supports the analytical finding in Sec. III B.

In addition to the above findings for the tribovoltaic current density as a function of the sliding speed, it is relevant to mention that the experimental results show a nearly linear increase in the short-circuit current versus the applied pressure [35, Fig. 10(b)]. The microscopic explanation behind this phenomenon is that the application of an external pressure increases the chance of carrier excitation through bond formation [35,37–39].

VII. CONCLUSIONS

A simple theory of tribovoltaics has been proposed based on the generation of electron-hole pairs when bonds are formed at the sliding surfaces. An estimate of the released energy in forming bonds at the surface has been formulated by solving a quantum mechanical two-potential problem. The formation of a bond may lead to the excitation of electron-hole pairs if the bonding-released energy is higher than the effective band gap at the semiconductor interface. An expression for the generation rate has been proposed to model tribovoltaic current transport in a p-n–doped semiconductor structure by solving the drift-diffusion equations supplemented by boundary and initial conditions. It has been shown analytically, and verified numerically using the COMSOL finite-element-method software, that the current density and carrier densities follow the time dependence of the sliding speed as long as the generated carrier concentrations are small compared to the background doping concentration.

ACKNOWLEDGMENTS

M.W. and Z.L.W. conceived of the project. M.W. constructed the analytical model. Z.Z. performed the numerical calculations. M.W., Z.Z., and Z.L.W. analyzed the results and wrote the manuscript. The authors declare no competing interests.

APPENDIX A: DEPLETION REGION ASSUMPTION

It is usual to propose analytically solvable models by assuming a depletion region near the p-n semiconductor interface and steady-state conditions. Here, we briefly outline the standard result about p-n structures, the approximation of a depletion zone, and the current density as a function of the applied bias voltage. The p-n semiconductor interface is located at $x = 0$, with the p side to the left and the n side to the right of the semiconductor interface. Electrons from the n side diffuse to the p side, where they recombine with holes, and vice versa. The assumption is that from $x = -x_p$ to $x = x_n$ (the depletion region), all mobile carriers (electrons and holes) recombine such that the charge density is $-qN_A$ on the p side (from $-x_p$ to 0) and qN_D on the n side (from 0 to x_n). Then, the Poisson equation can be solved for the electric field:

$$\mathcal{E}(x) = -\frac{d\phi}{dx} = -\frac{qN_A(x + x_p)}{\epsilon}, \quad \text{for } -x_p \le x < 0, \tag{A1}$$

$$\mathcal{E}(x) = \frac{qN_D(x - x_n)}{\epsilon}, \quad \text{for } 0 < x \le x_n. \tag{A2}$$

The recombination rate of minority carriers is modeled as [40]

$$R_p = \frac{p_n - p_{n0}}{\tau_p}, \tag{A3}$$

$$R_n = \frac{n_p - n_{p0}}{\tau_n}. \tag{A4}$$

Neglecting carrier generation,

$$G_p = G_n = 0, \tag{A5}$$

the electron and hole continuity equations [Eqs. (7) and (8)] become, in the neutral regions outside the depletion region,

$$\frac{d^2p_n}{dx^2} - \frac{p_n - p_{n0}}{D_p\tau_p} = 0, \quad n \text{ side}, \tag{A6}$$

$$\frac{d^2n_p}{dx^2} - \frac{n_p - n_{p0}}{D_n\tau_n} = 0, \quad p \text{ side}. \tag{A7}$$

The latter differential equations supplemented by the standard boundary conditions,

$$p_n(x = x_R) \approx p_n(x = \infty) = p_{n0}, \tag{A8}$$

$$p_n(x_n) = p_{n0}e^{\frac{qV_{\text{apl}}}{k_BT}}, \tag{A9}$$

$$n_p(x = x_L) \approx n_p(x = -\infty) = n_{p0}, \tag{A10}$$

$$n_p(-x_p) = n_{p0}e^{\frac{qV_{\text{apl}}}{k_BT}}, \tag{A11}$$

can be solved to yield, for the current densities,

$$J_p(x_n) = -qD_p\frac{dp_n}{dx}\|_{x_n} = \frac{qD_pp_{n0}}{\sqrt{D_p\tau_p}}\left(e^{\frac{qV_{\text{apl}}}{k_BT}} - 1\right), \tag{A12}$$

$$J_n(-x_p) = qD_n\frac{dn_p}{dx}\|_{-x_p} = \frac{qD_nn_{p0}}{\sqrt{D_n\tau_n}}\left(e^{\frac{qV_{\text{apl}}}{k_BT}} - 1\right). \tag{A13}$$

Since the electron and hole current densities J_n and J_p are assumed to be constants in the depletion region, where carriers are neither generated nor recombined, the total current density becomes

$$J = J_p(x_n) + J_n(-x_p) = J_s\left(e^{\frac{qV_{\rm apl}}{k_BT}} - 1\right), \tag{A14}$$

$$J_s = \frac{qD_p p_{n0}}{\sqrt{D_p\tau_p}} + \frac{qD_n n_{p0}}{\sqrt{D_n\tau_n}}, \tag{A15}$$

where J_s is the saturation current density. Note that in the absence of an applied voltage, the total current density vanishes, since the generation rate is assumed to be zero everywhere in the structure.

APPENDIX B: BOUNDARY AND INITIAL CONDITIONS

The drift-diffusion equations [Eqs. (6)–(8)] are solved numerically in COMSOL using the parameters in Table I subject to the boundary conditions given by Eqs. (9) and (10) where the applied voltage $V_{\rm apl}$ is fixed to zero. For the case of a time-dependent sliding speed, $v = v_m \sin(\omega_0 t)$, the initial conditions are chosen to correspond to the steady-state case in the absence of sliding excitation.

TABLE I. The table of parameters for GaAs [41] used in the numerical solution of the drift-diffusion equations.

Parameters	Expression	Description
L	5 (μm)	Length of the model
X_L	$-L$	p-n junction left boundary (p side)
X_R	L	p-n junction right boundary (n side)
A	4×10^{-12} (m^2)	Cross-section area of the model
κ	2	Crystal structure factor
α	5.64 (Å)	Lattice constant
$\eta_{eh\ \rm pair}$	1	Probability of electron-hole pair generation
T_m	$\frac{\kappa}{a^2}\eta_{eh\,\rm pair}$	Material-dependent function
μ_n	8500 [cm^2/(V s)]	Electron mobility
μ_p	400 [cm^2/(V s)]	Hole mobility
T	300 (K)	Temperature
k_B	1.38×10^{-23} (J/K)	Boltzmann's constant
q	1.6×10^{-19} (C)	Unit charge
N_a	10^{15} (1/cm^3)	Acceptor concentration
N_d	10^{15} (1/cm^3)	Donor concentration
ε_r	12.9	Relative dielectric constant
E_{g0}	1.424 (eV)	Band gap
χ_0	4.07 (eV)	Electron affinity
n_i	1×10^6 (1/cm^3)	Intrinsic carrier concentration
N_c	$n_i e^{\frac{E_{g0}}{2k_BT}}$	Conduction-band density of states
N_v	$n_i e^{\frac{E_{g0}}{2k_BT}}$	Valence-band density of states
τ_n	10^{-8} (s)	Electron lifetime
τ_p	10^{-8} (s)	Hole lifetime
D_n	$\frac{k_BT}{q}\mu_n$	Electron diffusion coefficient
D_p	$\frac{k_BT}{q}\mu_p$	Hole diffusion coefficient
σ	$L/100$	Gaussian-function standard deviation
$\delta(x)$	$\approx\frac{1}{\sqrt{2\pi\sigma^2}}e^{-\frac{x^2}{2\sigma^2}}$	Gaussian-distribution description of Dirac delta function

APPENDIX C: ENERGY RELEASE DUE TO BONDING FORMATION

Consider two surface atoms in materials A and B, respectively. The use of a one-electron model allows us to write, for the one-dimensional Hamiltonian of an electron moving in the combined surface potential of materials A and B,

$$H = \frac{p_z^2}{2m_0} + V_A(z - z_A) + V_B(z - z_B), \tag{C1}$$

where m_0 is the free-electron mass and $V_A(z - z_A)$ is the potential centered at $z = z_A$, where the latter defines the surface position of material A. Similarly, $V_B(z - z_B)$ is the potential centered at $z = z_B$, where the latter defines the surface position of material B. Hence, the surfaces of materials A and B are in the x-y plane and z denotes the position of the electron in the direction perpendicular to the material surfaces.

Let us introduce the isolated material Hamiltonians,

$$H_A = \frac{p_z^2}{2m_0} + V_A(z - z_A), \tag{C2}$$

$$H_B = \frac{p_z^2}{2m_0} + V_B(z - z_B), \tag{C3}$$

$$H_A|\psi_A\rangle = E_A|\psi_A\rangle, \tag{C4}$$

$$H_B|\psi_B\rangle = E_B|\psi_B\rangle, \tag{C5}$$

and write, for the total wave function describing a bonding state of an electron shared between materials A and B,

$$H|\psi\rangle = \mathcal{E}|\psi\rangle, \tag{C6}$$

$$|\psi\rangle = \alpha|\psi_A\rangle + \beta|\psi_B\rangle, \tag{C7}$$

where the latter expression can be written out as

$$\psi(z) = \alpha\psi_A(z - z_A) + \beta\psi_B(z - z_B). \tag{C8}$$

Above, E_A (E_B) are the energies of an electron bound to the isolated surface of material A (B), $\mathcal{E}$ is the energy of an electron shared between materials A and B, and α and β are coefficients to be determined. The corresponding wave functions are $|\psi_A\rangle$ and $|\psi_B\rangle$ for the isolated materials and $|\psi\rangle$ for an electron shared between materials A and B. Note that

$$H = H_A + V_B(z - z_B) = H_B + V_A(z - z_A). \tag{C9}$$

In order to determine the energy $\mathcal{E}$ of a shared electron, we use Eqs. (C8) and (C9) and compute the matrix element formed by multiplying with $\langle\psi_A(z - z_A)|$ from the left on $H|\psi(z)\rangle$,

$$\begin{aligned}\langle\psi_A(z - z_A)|H|\psi(z)\rangle &= \alpha\langle\psi_A(z - z_A)|H|\psi_A(z - z_A)\rangle + \beta\langle\psi_A(z - z_A)|H|\psi_B(z - z_B)\rangle \\ &= \alpha\langle\psi_A(z - z_A)|H_A|\psi_A(z - z_A)\rangle + \alpha\langle\psi_A(z - z_A)|V_B(z - z_B)|\psi_A(z - z_A)\rangle \\ &+ \beta\langle\psi_A(z - z_A)|H_B|\psi_B(z - z_B)\rangle + \beta\langle\psi_A(z - z_A)|V_A(z - z_A)|\psi_B(z - z_B)\rangle \\ &= \alpha E_A + \alpha s_{ABA} + \beta E_B r_{AB} + \beta t_{AAB} = \mathcal{E}\alpha + \mathcal{E}\beta r_{AB},\end{aligned} \tag{C10}$$

where, in the third step, the overlap integrals,

$$s_{ABA} = \langle\psi_A(z - z_A)|V_B(z - z_B)|\psi_A(z - z_A)\rangle, \tag{C11}$$

$$t_{AAB} = \langle\psi_A(z - z_A)|V_A(z - z_A)|\psi_B(z - z_B)\rangle, \tag{C12}$$

$$r_{AB} = \langle\psi_A(z - z_A)|\psi_B(z - z_B)\rangle, \tag{C13}$$

have been introduced, and in the fourth step, Eq. (C6) has been used. From the latter expression in Eq. (C10), collecting terms proportional to α and β yields

$$\alpha\,(E_A + s_{ABA} - \mathcal{E}) + \beta\,(E_B r_{AB} + t_{AAB} - \mathcal{E} r_{AB}) = 0. \tag{C14}$$

The other matrix element to be computed is formed by multiplying with $\langle\psi_B(z - z_B)|$ from the left on $H|\psi(z)\rangle$,

$$\begin{aligned}\langle\psi_B(z - z_B)|H|\psi(z)\rangle &= \alpha\langle\psi_B(z - z_B)|H|\psi_A(z - z_A)\rangle + \beta\langle\psi_B(z - z_B)|H|\psi_B(z - z_B)\rangle \\ &= \alpha\langle\psi_B(z - z_B)|H_A|\psi_A(z - z_A)\rangle + \alpha\langle\psi_B(z - z_B)|V_B(z - z_B)|\psi_A(z - z_A)\rangle \\ &+ \beta\langle\psi_B(z - z_B)|H_B|\psi_B(z - z_B)\rangle + \beta\langle\psi_B(z - z_B)|V_A(z - z_A)|\psi_B(z - z_B)\rangle \\ &= \alpha E_A r_{BA} + \alpha t_{BBA} + \beta E_B + \beta s_{BAB} = \mathcal{E}\alpha r_{BA} + \mathcal{E}\beta,\end{aligned} \tag{C15}$$

where, in the third step, the overlap integrals,

$$s_{BAB} = \langle \psi_B(z - z_B) | V_A(z - z_A) | \psi_B(z - z_B) \rangle, \tag{C16}$$

$$t_{BBA} = \langle \psi_B(z - z_B) | V_B(z - z_B) | \psi_A(z - z_A) \rangle, \tag{C17}$$

$$r_{BA} = \langle \psi_B(z - z_B) | \psi_A(z - z_A) \rangle, \tag{C18}$$

and, in the fourth step, Eq. (C6), have been used. From the latter expression, collecting terms proportional to α and β yields

$$\alpha \left(E_A r_{BA} + t_{BBA} - \mathcal{E} r_{BA} \right) + \beta \left(E_B + s_{BAB} - \mathcal{E} \right) = 0. \tag{C19}$$

Equations (C14) and (C19) can be written as a 2×2 matrix equation in the coefficients α and β:

$$\begin{bmatrix} E_A + s_{ABA} - \mathcal{E} & r_{AB} \left(E_B - \mathcal{E} \right) + t_{AAB} \\ r_{BA} \left(E_A - \mathcal{E} \right) + t_{BBA} & E_B + s_{BAB} - \mathcal{E} \end{bmatrix} \begin{bmatrix} \alpha \\ \beta \end{bmatrix} = \begin{bmatrix} 0 \\ 0 \end{bmatrix}. \tag{C20}$$

Solving the determinental equation for $\mathcal{E}$ corresponding to Eq. (C20),

$$\begin{aligned} & K_0 \mathcal{E}^2 + K_1 \mathcal{E} + K_2 = 0, \\ & K_0 = 1 - r_{AB} r_{BA}, \\ & K_1 = r_{AB} r_{BA} \left(E_A + E_B \right) + r_{BA} t_{AAB} + r_{AB} t_{BBA} \\ & \quad - \left(E_A + E_B + S_{ABA} + S_{BAB} \right), \\ & K_2 = \left(E_A + S_{ABA} \right) \left(E_B + S_{BAB} \right) \\ & \quad - r_{AB} r_{BA} E_A E_B - t_{AAB} r_{BA} E_A - t_{BBA} r_{AB} E_B - t_{AAB} t_{BBA}, \end{aligned} \tag{C21}$$

gives the possible eigenvalues for a bonding electron,

$$\mathcal{E} = \frac{-K_1 \pm \sqrt{K_1^2 - 4 K_0 K_2}}{2 K_0}. \tag{C22}$$

Note that since the potentials V_A and V_B are real, and the wave functions $|\psi_A\rangle, |\psi_B\rangle$ can be chosen real, the following identities hold:

$$\begin{aligned} r_{BA} &= r_{BA}^* = r_{AB}, \\ t_{AAB} &= t_{AAB}^* = t_{BAA}, \\ s_{ABA} &= s_{ABA}^*, \\ t_{BBA} &= t_{BBA}^* = t_{ABB}, \\ s_{BAB} &= s_{BAB}^*. \end{aligned}$$

[1] Z. L. Wang, in *Handbook of Triboelectric Nanogenerators*, Vol. 1, edited by Zhong Lin Wang, Ya Yang, Junyi Zhai, and Jie Wang (Springer, Cham, Switzerland, 2023), Chapter 1.

[2] G. Zhu, C. Pan, W. Guo, C.-Y. Chen, Y. Zhou, R. Yu, and Z. L. Wang, Triboelectric-generatordriven pulse electrodeposition for micropatterning, Nano Lett. **12**, 4960 (2012).

[3] G. Zhu, J. Chen, Y. Liu, P. Bai, Y. S. Zhou, Q. Jing, C. Pan, and Z. L. Wang, Linear-grating triboelectric generator based on sliding electrification, Nano Lett. **13**, 2282 (2013).

[4] S. Wang, Y. Xie, S. Niu, L. Lin, and Z. L. Wang, Freestanding triboelectric-layer-based nanogenerators for harvesting energy from a moving object or human motion in contact and noncontact modes, Adv. Mater. **26**, 2818 (2014).

[5] J. Gravesen, M. Willatzen, J. Shao, and Z. L. Wang, Energy optimization of a mirror-symmetric spherical triboelectric nanogenerator, Adv. Funct. Mater. **32**, 2110516 (2022).

[6] J. Gravesen, M. Willatzen, J. Shao, and Z. L. Wang, in *Handbook of Triboelectric Nanogenerators*, Vol. 1, edited by Zhong Lin Wang, Ya Yang, Junyi Zhai, and Jie Wang (Springer, Cham, Switzerland, 2023), Chapter 6.

[7] Y. Yang, Y. S. Zhou, H. Zhang, Y. Liu, S. Lee, and Z. L. Wang, A single electrode based triboelectric nanogenerator as self-powered tracking system, Adv. Mater. **25**, 6594 (2013).

[8] S. Lin and Z. L. Wang, The tribovoltaic effect, Mater. Today **62**, 111 (2023).

[9] M. Zheng, S. Lin, L. Zhu, Z. Tang, and Z. L. Wang, Effects of temperature on the tribovoltaic effect at liquid-solid interfaces, Adv. Mater. Interfaces **9**, 2101757 (2022).

[10] M. Zheng, S. Lin, Z. Tang, Y. Feng, and Z. L. Wang, Photovoltaic effect and tribovoltaic effect at liquid-semiconductor interface, Nano Energy **83**, 105810 (2021).

[11] S. Lin, X. Chen, and Z. L. Wang, Contact electrification at the liquid-solid interface, Chem. Rev. **122**, 5209 (2022).

[12] C. Xu, J. Yu, Z. Huo, Y. Wang, Q. Sun, and Z. L. Wang, Pursuing the tribovoltaic effect for direct-current triboelectric nanogenerators, Energy Environ. Sci. **16**, 983 (2023).

[13] S. Sriphan and N. Vittayakorn, Tribovoltaic effect: Fundamental working mechanism and emerging applications, Mater. Today Nano **22**, 100318 (2023).

[14] Z. Zhang, D. Jiang, J. Zhao, G. Liu, T. Bu, C. Zhang, and Z. L. Wang, Tribovoltaic effect on metal-semiconductor interface for direct-current low-impedance triboelectric nanogenerators, Adv. Energy Mater. **10**, 1903713 (2020).

[15] Z. Chen, Y. Lin, Y. Lv, H. Zhou, W. Sun, and C. Zhang, Friction-dominated carrier excitation and transport mechanism for GaN-based direct-current triboelectric nanogenerators, ACS Appl. Mater. Interfaces **14**, 24020 (2022).

[16] Z. Z. Wang, Z. Zhang, Y. K. Chen, L. K. Gong, S. C. Dong, H. Zhou, Y. Lin, Y. Lv, G. X. Liu, and C. Zhang, Achieving an ultrahigh direct-current voltage of 130 V by semiconductor heterojunction power generation based on the tribovoltaic effect, Energy Environ. Sci. **15**, 2366 (2022).

[17] Z. Zhang, Z. Wang, Y. Chen, Y. Feng, S. Dong, H. Zhou, Z. L. Wang, and C. Zhang, Semiconductor contact-electrification-dominated tribovoltaic effect for ultrahigh power generation, Adv. Mater. **34**, e2200146 (2022).

[18] W. F. Pasveer, J. Cottaar, C. Tanase, R. Coehoorn, P. A. Bobbert, P. W. M. Blom, D. D. de Leuw, and M. A. J.

Micehls, Unified description of charge-carrier mobilities in disordered semiconducting polymers, Phys. Rev. Lett. **94**, 206601 (2005).
[19] J. A. Röhr and R. C. I. MacKenzie, Analytical description of mixed ohmic and space-charge-limited conduction in single-carrier devices, J. Appl. Phys. **128**, 165701 (2020).
[20] J. X. Sun, H. Ch. Yang, Y. Li, and H. J. Cui, Unified mobility model for diffusion-limited current in organic diodes based on Fermi-Dirac statistics, Phys. Rev. Appl. **16**, 034037 (2021).
[21] J. X. Sun, H. Ch. Yang, Y. Li, and H. J. Cui, Analytic solutions of drift-diffusion equations and mobility of organic semiconductors, Phys. Rev. Appl. **20**, 034061 (2023).
[22] M. Benaichi, A. Chetouani, A. Karkri, D. Moussaid, and S. E. Elqabbaj, Three-dimensional drift-diffusion model for simulation and investigation of bordering effects in silicon solar cells, Mater. Today Proc. **13**, 630 (2019).
[23] T. Golubev, D. Liu, R. Lunt, and P. Duxbury, Understanding the impact of C60 at the interface of perovskite solar cells via drift-diffusion modeling, AIP Adv. **9**, 035026 (2019).
[24] T. S. Sherkar, C. Momblona, L. Gil-Escrif, H. J. Bolink, and L. J. A. Koster, Improving perovskite solar cells: Insights from a validated device model, Adv. Energy Mater. **7**, 1602432 (2017).
[25] S. Selberherr, *Analysis and Simulation of Semiconductor Devices* (Springer-Verlag, Wien, New York, 1984).
[26] H. Gummel, A self-consistent iterative scheme for one-dimensional steady state transistor calculations, IEEE Trans. Electron. Devices **11**, 455 (1964).
[27] D. Scharfetter and H. Gummel, Large-signal analysis of a silicon Read diode oscillator, IEEE Trans. Electron. Devices **16**, 64 (1969).
[28] J. Mørk, M. Willatzen, J. Mark, M. Preisel, and C. P. Seltzer, Characterization and modelling of ultrafast carrier dynamics in quantum well optical amplifiers, SPIE **2146**, 52 (1994).
[29] Z. L. Wang and A. C. Wang, On the origin of contact electrification, Mater. Today **30**, 34 (2019).
[30] S. G. Davison and M. Steslicka, *Basic Theory of Surface States*, Monographs on the Physics and Chemistry of Materials, Vol. 46 (Oxford Science Publications, Oxford, 2008).
[31] G. Bastard, *Wave Mechanics Applied to Semiconductor Heterostructures*, Monographies de Physique (Halsted Press, 1988).
[32] M. Willatzen, L. C. Lew Yan Voon, and Z. L. Wang, Quantum theory of contact electrification for fluids and solids, Adv. Funct. Mater. **30**, 1910461 (2020).
[33] H. Haug and S. W. Koch, *Quantum Theory of the Optical and Electronic Properties of Semiconductors* (World Scientific, NJ, 2003).
[34] W. A. Harrison, *Electronic Structure and the Properties of Solids* (Dover Publications, Mineola, New York, USA, 1989).
[35] R. Xu, Q. Zhang, J. Y. Wang, D. Liu, J. Wang, and Z. L. Wang, Direct current triboelectric cell by sliding an *n*-type semiconductor on a *p*-type semiconductor, Nano Energy **66**, 104185 (2019).
[36] L. C. Lew Yan Voon and M. Willatzen, *The $k \cdot p$ Method* (Springer, Berlin, Heidelberg, Germany, 2009).
[37] D. Yang, L. Zhang, N. Luo, Y. Liu, W. Sun, J. Peng, M. Feng, Y. Feng, H. Wang, and D. Wang, Tribological-behaviour-controlled direct-current triboelectric nanogenerator based on the tribovoltaic effect under high contact pressure, Nano Energy **99**, 107370 (2022).
[38] Y. Lu, Z. Hao, S. Feng, R. Shen, Y. Yan, and S. Lin, Direct-current generator based on dynamic PN junctions with the designed voltage output, iScience **22**, 58 (2019).
[39] X. Huang, X. Xiang, J. Nie, D. Peng, F. Yang, Z. Wu, H. Jiang, Z. Xu, and Q. Zheng, Microscale Schottky superlubric generator with high direct-current density and ultralong life, Nat. Commun. **12**, 2268 (2021).
[40] S. M. Sze, *Semiconductor Devices—Physics and Technology* (John Wiley & Sons, New York, 1985).
[41] J. S. Blakemore, Semiconducting and other major properties of gallium arsenide, J. Appl. Phys. **53**, R123 (1982).

Correction: An incorrect version of Figure 8 was used for publication and has now been replaced with the correct version.